

Green exciton series in cuprous oxide

Patric Rommel,* Patrik Zielinski, and Jörg Main

Institut für Theoretische Physik 1, Universität Stuttgart, 70550 Stuttgart, Germany

(Dated: February 19, 2020)

We numerically investigate the odd parity states of the green exciton series in cuprous oxide. Taking into account the coupling to the yellow series and especially to the yellow continuum, the green excitons are quasi-bound resonances with a finite lifetime which cannot be described with Hermitian operators. To calculate their positions and linewidths, we use the method of complex-coordinate rotation, leading to a non-Hermitian complex eigenvalue problem. We find that the behavior of the dominant P states is very well approximated by a modified Rydberg formula using a negative quantum defect. The corresponding linewidths induced by the coupling to the yellow continuum decrease with the third power of the principal quantum number.

I. INTRODUCTION

Early experiments on cuprous oxide in the 1950s were able to observe excitons with principal quantum numbers up to $n = 9$ [1]. Since then, experimental methods have made tremendous progress. After Kazimierzczuk *et al.* realized principal quantum numbers up to $n = 25$ for the yellow series in cuprous oxide [2], interest has been drawn to the field of giant Rydberg excitons. Due to the influence of the crystal symmetry, the exciton sequence shows deviations from a perfect hydrogen-like spectrum. For example, a splitting of the P and F states is observable [3, 4].

In an idealized model, excitons can be described as bound states between electrons and holes. In general, a range of mechanisms make scattering possible and induce a finite linewidth. The excitons become quasi-bound states or resonances. In case of the yellow excitons, the most prominent process is the scattering with phonons [5, 6]. Bound states can also become resonances by application of an external electric field, which allows for tunneling processes into the unbound region [7, 8].

In cuprous oxide, the excitons constituted by electrons in the lowest conduction Γ_6^+ band and holes in the highest Γ_7^+ valence band are part of the yellow exciton series. An electron can also be lifted from the Γ_8^+ valence band into the Γ_6^+ conduction band, forming a green exciton [9–11]. Since the energy of the Γ_8^+ valence band is lowered by an amount Δ in comparison to the uppermost Γ_7^+ valence band, all green excitons, except for the even parity 1S states investigated in [12, 13], lie within the energy range of the yellow continuum. Yellow and green states are coupled by the valence band structure [4, 14], and the green states with principal quantum numbers $n \geq 2$ are therefore resonances instead of truly bound states.

An efficient numerical method for the computation of the bound states of Cu_2O including the impact of the valence band structure (but ignoring the phonon coupling) is the diagonalization of the Hamiltonian using a complete basis set [4, 13]. The method can be applied to

obtain the bound states of the yellow exciton series at energies below the gap energy $E_g = 2.17208\text{ eV}$ and the green 1S excitons, which are the only bound states of the green exciton series. However, the Hermitian eigenvalue problem does not allow for the computation of unbound resonance states.

Recent work by Krüger and Scheel has focused on the interseries transitions such as between the yellow and green excitons [15]. A better understanding of the unbound resonances of the green series is thus of interest. A convenient description of these resonance states is achieved by the introduction of a complex energy, where the imaginary part is related to the linewidth of the quasi-bound state. These complex energies can be calculated by way of the complex-coordinate-rotation method [16–18], where a complex scaling operation is performed to expose the resonance positions in the complex plane. In this paper the numerical algorithm introduced in Refs. [4, 13] for the computation of bound excitons is augmented by application of the complex-coordinate rotation. This rotation turns the Hermitian eigenvalue problem into a non-Hermitian system, and thus allows, for the first time, for the computation of the complex resonance energies of the green excitons. To this end, we first introduce the necessary theory in Sec. II, including the method of complex-coordinate rotation and the exciton Hamiltonian, also giving a short discussion of the numerical diagonalization and the extraction of the oscillator strengths. In Sec. III we present our numerical results and discuss their implications. Finally, we draw conclusions and give a brief outlook in Sec. IV.

II. THEORY

Both the yellow and the green series in Cu_2O have a unified description in terms of the Hamiltonian [4, 14, 19]

$$H = E_g + H_e(\mathbf{p}_e) + H_h(\mathbf{p}_h) + V(\mathbf{r}_e - \mathbf{r}_h). \quad (1)$$

Here, E_g denotes the gap energy, H_e and H_h are the electron and hole kinetic energies, and V is the screened

* Email: patric.rommel@itp1.uni-stuttgart.de

Coulomb potential

$$V(\mathbf{r}_e - \mathbf{r}_h) = -\frac{e^2}{4\pi\epsilon_0\epsilon|\mathbf{r}_e - \mathbf{r}_h|}, \quad (2)$$

with the dielectric constant ϵ . The electron and hole kinetic energies are given by

$$H_e(\mathbf{p}_e) = \frac{\mathbf{p}_e^2}{2m_e}, \quad (3)$$

$$\begin{aligned} H_h(\mathbf{p}_h) = & H_{\text{SO}} + \frac{1}{2\hbar^2 m_0} \{ \hbar^2(\gamma_1 + 4\gamma_2)\mathbf{p}_h^2 \\ & + 2(\eta_1 + 2\eta_2)\mathbf{p}_h^2(\mathbf{I} \cdot \mathbf{S}_h) \\ & - 6\gamma_2(p_{h1}^2 \mathbf{I}_1^2 + \text{c.p.}) - 12\eta_2(p_{h1}^2 \mathbf{I}_1 \mathbf{S}_{h1} + \text{c.p.}) \\ & - 12\gamma_3(\{p_{h1}, p_{h2}\}\{\mathbf{I}_1, \mathbf{I}_2\} + \text{c.p.}) \\ & - 12\eta_3(\{p_{h1}, p_{h2}\}(\mathbf{I}_1 \mathbf{S}_{h2} + \mathbf{I}_2 \mathbf{S}_{h1}) + \text{c.p.}) \}, \quad (4) \end{aligned}$$

with m_e and m_0 the effective and free electron mass, respectively, $\{a, b\} = \frac{1}{2}(ab + ba)$ the symmetrized product, and c.p. denotes cyclic permutation. The spin-orbit interaction

$$H_{\text{SO}} = \frac{2}{3}\Delta \left(1 + \frac{1}{\hbar^2} \mathbf{I} \cdot \mathbf{S}_h \right), \quad (5)$$

ouples the hole spin \mathbf{S}_h and the quasispin \mathbf{I} introduced to describe the degeneracy of the valence band Bloch functions. The yellow and green series are split by the energy Δ . The parameters η_j and the three Luttinger parameters γ_j parameterize the influence of the complex band structure and the deviation from a parabolic dispersion relation. In contrast to Refs. [13, 20] we here focus on odd excitons and thus can neglect the central-cell corrections. Finally, the Hamiltonian (1) is transformed into relative and center-of-mass coordinates [21],

$$\begin{aligned} \mathbf{r} = \mathbf{r}_e - \mathbf{r}_h, \quad \mathbf{R} = \frac{m_h \mathbf{r}_h + m_e \mathbf{r}_e}{m_h + m_e}, \\ \mathbf{P} = \mathbf{p}_e + \mathbf{p}_h, \quad \mathbf{p} = \frac{m_h \mathbf{p}_e - m_e \mathbf{p}_h}{m_h + m_e}, \quad (6) \end{aligned}$$

with vanishing center-of-mass momentum $\mathbf{P} = 0$. The material parameters for Cu_2O are given in Table I.

The yellow exciton series in cuprous oxide can now be investigated as in our previous work [4, 13] by diagonalizing the resulting Hamiltonian (1). States lying above the band gap energy $E_g = 2.17208$ eV on the other hand are resonances not accessible by this method. For their study, in this paper we augment the approach by the complex-coordinate rotation [16–18], allowing for the calculation of the complex energies of the green exciton states. The wave functions ψ associated with resonances are not normalizable and thus are not part of the Hilbert space. They fulfill the Schrödinger equation

$$H\psi = E\psi \quad (7)$$

with a complex energy E . We introduce the complex scaling operation S_θ with

$$S_\theta \psi(\mathbf{r}) = \psi(\mathbf{r}e^{i\theta}). \quad (8)$$

Note that formally the operator S_θ can be applied to a state $|\psi\rangle$ in arbitrary representation, however, Eq. (8) is only valid in coordinate representation as used throughout this paper. For sufficiently large θ , $S_\theta \psi$ becomes square integrable [18]. The rotated Schrödinger equation is given by

$$S_\theta H S_\theta^{-1} S_\theta \psi = E S_\theta \psi. \quad (9)$$

We thus want to find eigenvalues and normalizable eigenfunctions of the rotated Hamiltonian

$$H' = S_\theta H S_\theta^{-1}. \quad (10)$$

The energies of the bound states are unaffected by the rotation, whereas the continuum is rotated into the lower complex plane by the angle 2θ and the positions of the quasi-bound resonance states are revealed. For sufficiently large angles, these are independent of the value of θ . Expressing $S_\theta \psi$ in a basis $\{\phi_i\}$, we obtain

$$S_\theta |\psi\rangle = \sum_i c_i |\phi_i\rangle \quad (11)$$

and

$$\sum_i \langle \phi_j | S_\theta^{-1} H S_\theta^{-1} | \phi_i \rangle c_i = E \sum_i \langle \phi_j | S_\theta^{-1} S_\theta^{-1} | \phi_i \rangle c_i. \quad (12)$$

The solution can thus be obtained by using the rotated basis set $\{S_\theta^{-1} |\phi_i\rangle\}$ with the unchanged Hamiltonian H .

We now express the wave function in an appropriate basis. Our approach is identical to the one in Ref. [8], i.e., for the radial part, we use the complete basis of Coulomb-Sturmian functions

$$U_{NL}(\rho) = N_{NL}(2\rho)^L e^{-\rho} L_N^{2L+1}(2\rho), \quad (13)$$

with $\rho = r/\alpha$ and N the radial quantum number. Here, α is a free parameter. For the angular part we use the

TABLE I. Material parameters of Cu_2O used in the calculations.

Energy gap	$E_g = 2.17208$ eV	[2]
Spin-orbit coupling	$\Delta = 0.131$ eV	[22]
Effective electron mass	$m_e = 0.99m_0$	[23]
Effective hole mass	$m_h = 0.58m_0$	[23]
Dielectric constant	$\epsilon = 7.5$	[24]
Valence band parameters	$\gamma_1 = 1.76$	[22]
	$\gamma_2 = 0.7532$	[22]
	$\gamma_3 = -0.3668$	[22]
	$\eta_1 = -0.020$	[22]
	$\eta_2 = -0.0037$	[22]
	$\eta_3 = -0.0337$	[22]

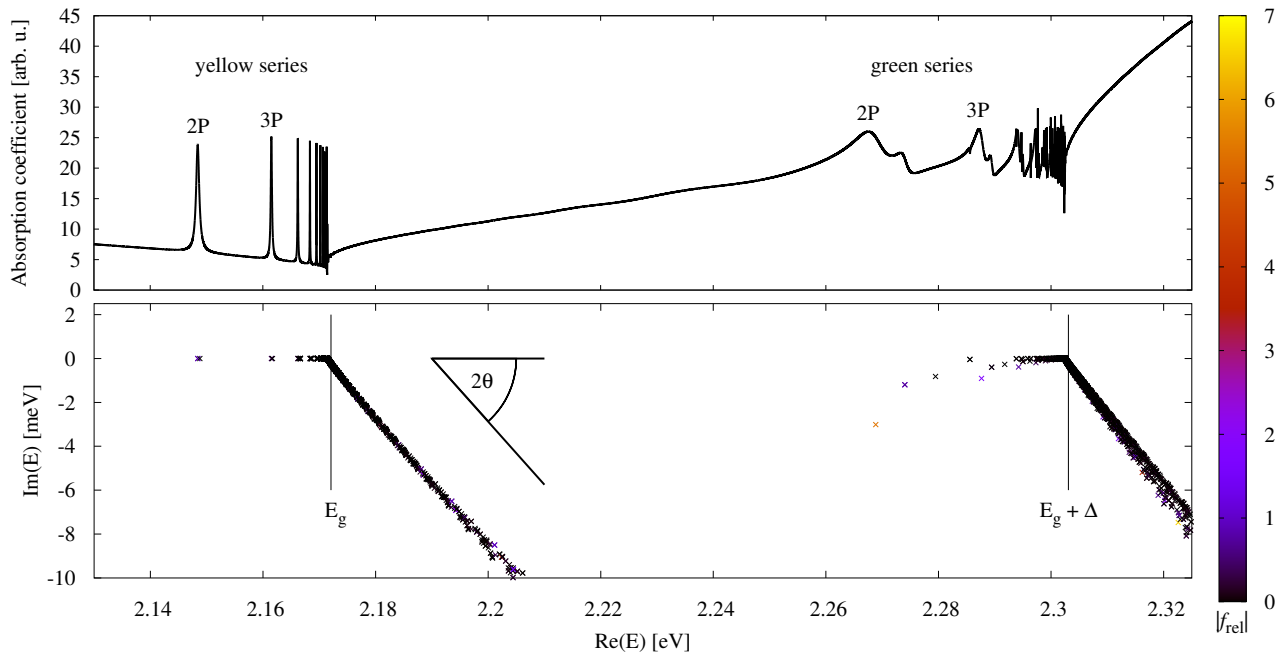


FIG. 1. Spectrum and resonance positions in the complex plane for the yellow and green exciton series of Cu_2O . Note that only the odd parity states are included. The color bar shows the absolute value of the relative oscillator strength $|f_{\text{rel}}|$. As coupling with phonons is not considered here, the linewidths of the yellow exciton states in the upper panel were put in by hand, as explained in the text. The vertical lines mark the respective band gaps. Due to the finite basis, the numerical resonance positions are already rotated into the lower complex plane at a slightly lower energies. The absorption coefficient is given in arbitrary units and with an arbitrary shift of the base line.

spherical harmonics for L with an additional set of appropriate spin quantum numbers. First, the quasispin I and the hole spin S_h are coupled to the effective hole spin J . At the Γ point, J is a good quantum number and distinguishes between the yellow ($J = 1/2$) and green series ($J = 3/2$). Then L and J are coupled to the angular momentum F . Finally, we take the electron spin into account by introducing $F_t = F + S_e$ with the component M_{F_t} along the quantization axis, which is chosen to be the [001] axis. Our basis states thus are given by

$$|\Pi\rangle = |N, L; (I, S_h), J, F, S_e; F_t, M_{F_t}\rangle. \quad (14)$$

Using this basis set, we can transform the Schrödinger equation into the generalized eigenvalue problem (12), which can be solved using the Lapack routine ZGGEV [25]. The complex-coordinate rotation is here achieved by rotating the free parameter $\alpha \rightarrow \alpha = |\alpha|e^{i\theta}$. Since the Coulomb-Sturmian functions are not orthogonal, the overlap matrix in Eq. (12) is nontrivial [4]. To properly orthonormalize the eigenvectors, we apply a modified Gram-Schmidt procedure.

Using the eigenfunctions obtained from the solution of the generalized eigenvalue problem (12), we are able to simulate absorption spectra for the yellow and green series. The absorption coefficients are calculated with

the formula [8]

$$f(E) = -\frac{1}{\pi} \text{Im} \sum_j \frac{f_{\text{rel}}^{(j)}}{E - E_j}, \quad (15)$$

where E_j are the complex energies of the resonance states and

$$f_{\text{rel}} \sim \left(\lim_{r \rightarrow 0} \frac{\partial}{\partial r} \langle \sigma_z^\pm | \Psi(\mathbf{r}) \rangle \right)^2 \quad (16)$$

is the complex generalization of the relative oscillator strength. The overlaps with the states

$$\begin{aligned} |\sigma_z^+\rangle &= |2, -1\rangle_D, \\ |\sigma_z^-\rangle &= |-2, 1\rangle_D, \end{aligned} \quad (17)$$

determine the spectrum for σ^+ and σ^- polarized light. Here, we use the abbreviation

$$\begin{aligned} |F_t, M_{F_t}\rangle_D &= |(S_e, S_h) S, I; I + S, L; F_t, M_{F_t}\rangle \\ &= |(1/2, 1/2) 0, 1; 1, 1; F_t, M_{F_t}\rangle, \end{aligned} \quad (18)$$

to denote the states with a coupling scheme differing from the one in the basis states.

III. RESULTS AND DISCUSSION

The results for both the yellow and green exciton series are presented in Fig. 1. In the computations we have

used the basis set (14) with $N + L < 50$, $|\alpha| = 63$, and $\theta = 0.14$ and restricted ourselves to the odd states, as only those contribute to the absorption coefficient of one-photon transitions. In the lower part of Fig. 1 we show the resonance positions of the yellow and green exciton series in the complex energy plane. Clearly visible are the bound states of the yellow exciton series at energies below the gap energy E_g and the resonances of the green exciton series at energies below the band edge $E_g + \Delta$. Above the band edges energies are bundled along straight lines and rotated into the complex plane. The rotation angle is nearly given by 2θ as is expected for complex rotated continuum states [16–18]. Note that the numerical resonance positions are already rotated into the lower complex energy plane at energies slightly below the band edges. This is a numerical artifact due to the finite size of the basis set.

The upper part of Fig. 1 presents the corresponding absorption spectrum obtained with Eq. (15). Since we do not include the effects of phonons in our model, the yellow exciton states here are bound states with infinite lifetimes. To avoid δ function type absorption peaks we have simulated the interaction with phonons by manually introducing the finite linewidths

$$\gamma_n = 9 \text{ meV}(n^2 - 1)/n^5 \quad (19)$$

with an effective principal quantum number

$$n = \sqrt{E_{\text{Ryd}}/(E_g - E)} + \delta_P \quad (20)$$

derived from the approximate Rydberg formula [2, 6] with $E_{\text{Ryd}} = 92 \text{ meV}$ and $\delta_P = 0.23$.

The green exciton states, however, are true resonances even apart from phonons, since they are coupled to the yellow continuum by the valence band structure. The linewidths visible in the upper part of Fig. 1 are solely due to this effect. The continuum states of both the yellow and green excitons provide for a square root function shaped background starting at energies above the respective band edges.

We now want to discuss the classification and symmetries of resonances of the green exciton series. The green excitons are defined by the condition $J = 3/2$. Additionally, we have to consider the angular momentum L . The electron spin plays no role for the odd states and remains a good quantum number. Thus, for the P states we have $F = 1/2, 3/2$, and $5/2$. Reducing the symmetry to the octahedral group O_h , the irreducible representations are Γ_6^- , Γ_8^- , and $\Gamma_7^- \oplus \Gamma_8^-$, respectively [26]. We have to take into account, however, that the quasispin I transforms according to Γ_5^+ instead of Γ_4^+ . Since $\Gamma_5^+ = \Gamma_4^+ \otimes \Gamma_2^+$, this can be done by performing the coupling of angular momenta as usual, but multiplying by Γ_2^+ in the end. For the P states, we thus have the representations Γ_6^- , Γ_8^- , Γ_7^- , and Γ_8^- . Note that the degeneracy of these states is doubled due to the electron spin. Since half-integer angular momenta only have the above mentioned irreducible representations in O_h [26], all states considered in this

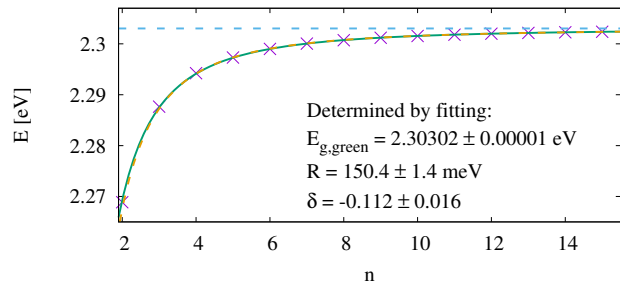


FIG. 2. Numerically determined energies of the lowest dominant P states. The band gap energy $E_{g,\text{green}}$, Rydberg constant R , and quantum defect δ are determined by a fit (green solid line). For comparison, the dashed yellow line shows a fit without quantum defect (see text).

work can be classified according to them. Of those, only Γ_6^- and Γ_8^- states are dipole active, because only those contain Γ_4^+ when multiplied with the electron spin symmetry Γ_6^+ [26]. Additional consideration of the degree of degeneracy then allows for the unique assignment of irreducible representations to the odd exciton states as given in the Supplemental Material [27].

In Table I and in Fig. 2 the resonance positions of the dominant P states are presented. We extract the band gap, Rydberg constant and quantum defect using a fit of the form $E(n) = E_g - R/(n - \delta)^2$. As expected, the fitted continuum threshold $E_{g,\text{green}}^{\text{fit}} = 2.30302 \text{ eV}$ shows excellent agreement with the band gap of the green excitons $E_g + \Delta = 2.30308 \text{ eV}$. For the Rydberg constant we obtain $R = 150.4 \text{ meV}$, which is in good agreement with literature [10, 12, 19, 28]. In previous theoretical work by Schöne *et al.* [19], the quantum defect of the green exciton series was investigated using a simplified treatment of the valence band dispersion neglecting the coupling of the green resonances to the yellow continuum, yielding

TABLE II. Numerically determined resonance positions of some of the lowest P states belonging to the irreducible representation Γ_6^- . The selected states produce the dominant peak of each n -manifold in the absorption spectrum.

State	Re E [eV]	Im E [meV]	Re f_{rel}	Im f_{rel}
2P	2.26887	-3.01965	4.2998	5.8604
3P	2.28765	-0.90691	1.1603	1.8982
4P	2.29423	-0.38575	0.5028	0.8270
5P	2.29731	-0.19095	0.2571	0.4496
6P	2.29901	-0.10700	0.1337	0.2630
7P	2.30005	-0.06821	0.1416	0.1579
8P	2.30072	-0.04328	0.0519	0.1085
9P	2.30120	-0.03314	0.0438	0.0730
10P	2.30154	-0.02334	0.0302	0.0550
11P	2.30180	-0.01733	0.0268	0.0387
12P	2.30199	-0.01459	0.0198	0.0322
13P	2.30215	-0.01012	0.0168	0.0223
14P	2.30227	-0.00903	0.0118	0.0212
15P	2.30237	-0.00742	0.0105	0.0165

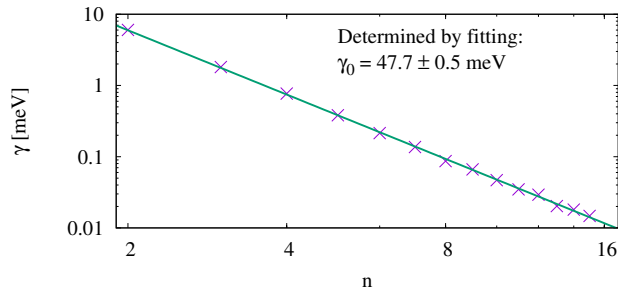


FIG. 3. The numerically determined yellow-continuum induced linewidths of the dominant green P states. A fit using the function $\gamma_n = \gamma_0 n^{-3}$ is in good agreement with the numerical data.

negative quantum defects, which for the P states are in reasonable agreement with our result of $\delta = -0.112$. In Fig. 2 we also present a fit without using a quantum defect. Detailed comparison shows that this fit is slightly less accurate, especially for low principal quantum numbers. This motivates the validity of the quantum-defect corrected Rydberg formula also for the dominant P states of the green exciton series. A more complete version of Table I is given in the Supplemental Material [27].

The green exciton series has already been experimentally investigated in Ref. [1]. At temperature $T = 4.2$ K Gross found $E_{2P} = 2.266$ eV, $E_{3P} = 2.287$ eV, $E_{4P} = 2.294$ eV and $E_{5P} = 2.298$ eV, which agrees with the numerical energies given in Table I to within approximately 1 - 2 meV.

The behavior of the linewidths of the green excitons induced by the coupling to the yellow continuum as a function of the principal quantum number is shown in Fig. 3. A function of the form $\gamma_n = \gamma_0 n^{-3}$ provides a good fit to the numerically determined values. We obtain $\gamma_0 = 47.7$ meV, which means that the yellow-continuum induced linewidths of the dominant green P states are large compared to the phonon-coupling induced linewidths of the yellow excitons given in Eq. (19). Assuming that the phonon-coupling leads to similar linewidths for both the yellow and green excitons, the widths of the green excitons shown in Fig. 1 would only slightly increase when taking phonon-coupling into account, however, a more detailed theory of the phonons or precise state-of-the-art

experimental data are necessary to clarify this point.

IV. CONCLUSION AND OUTLOOK

We have computed the resonance positions, linewidths, and relative oscillator strengths of the green exciton series of cuprous oxide, thereby taking into account the valence band structure of the crystal and the coupling of the green excitons to the yellow continuum. For the computations we have used a complete basis set with Coulomb-Sturmian functions for the radial part of the wave function and the complex-coordinate rotation method. For the dominant P states in the absorption spectrum we have confirmed their hydrogen-like behavior and extracted the Rydberg energy and quantum defect, which are in good agreement with literature [19]. The linewidths of the green P states decrease $\sim n^{-3}$ with increasing principal quantum number.

In Sec. III we have compared some resonance positions to the experimental work of Gross [1]. In the meantime experimental techniques have made substantial progress. A comparison with new data would thus be desirable. The interesting question is whether giant Rydberg states of the green exciton series with quantum numbers up to $n \approx 25$ and the computed fine structure splitting can be experimentally observed similar as for the yellow series [2, 3].

In this paper, we have focused on the odd states. The 1S state of the even green series is bound and has been computed, including the central-cell corrections, in Ref. [13]. In the future we can also investigate the even resonance states of the green exciton series.

Interseries transitions are currently investigated [15]. Starting from the present investigations, we can now go on to calculate the interseries transition amplitudes between the yellow and green series, taking the valence band structure into account.

ACKNOWLEDGMENTS

This work was supported by Deutsche Forschungsgemeinschaft (DFG) through Grant No. MA1639/13-1. We thank Frank Schweiner for his contributions and Günter Wunner for a careful reading of the manuscript.

-
- [1] E. F. Gross, *Il Nuovo Cimento* (1955-1965) **3**, 672 (1956).
 - [2] T. Kazimierczuk, D. Fröhlich, S. Scheel, H. Stolz, and M. Bayer, *Nature* **514**, 343 (2014).
 - [3] J. Thewes, J. Heckötter, T. Kazimierczuk, M. Aßmann, D. Fröhlich, M. Bayer, M. A. Semina, and M. M. Glazov, *Phys. Rev. Lett.* **115**, 027402 (2015).
 - [4] F. Schweiner, J. Main, M. Feldmaier, G. Wunner, and C. Uihlein, *Phys. Rev. B* **93**, 195203 (2016).

- [5] F. Schweiner, J. Main, and G. Wunner, *Phys. Rev. B* **93**, 085203 (2016).
- [6] H. Stolz, F. Schöne, and D. Semkat, *New Journal of Physics* **20**, 023019 (2018).
- [7] J. Heckötter, M. Freitag, D. Fröhlich, M. Aßmann, M. Bayer, M. A. Semina, and M. M. Glazov, *Phys. Rev. B* **98**, 035150 (2018).
- [8] P. Zielinski, P. Rommel, F. Schweiner, and J. Main, *J. Phys. B* **53**, 054004 (2020).

- [9] S. Nikitine, The Philosophical Magazine: A Journal of Theoretical Experimental and Applied Physics **4**, 1 (1959).
- [10] J. B. Grun, M. Sieskind, and S. Nikitine, J. Phys. Radium **22**, 176 (1961).
- [11] J. Grun and S. Nikitine, Journal de Physique **24**, 355 (1963).
- [12] C. Uihlein, D. Fröhlich, and R. Kenklies, Phys. Rev. B **23**, 2731 (1981).
- [13] F. Schweiner, J. Main, G. Wunner, and C. Uihlein, Phys. Rev. B **95**, 195201 (2017).
- [14] J. M. Luttinger, Phys. Rev. **102**, 1030 (1956).
- [15] S. O. Krüger and S. Scheel, Phys. Rev. B **100**, 085201 (2019).
- [16] W. P. Reinhardt, Annual Review of Physical Chemistry **33**, 223 (1982).
- [17] Y. K. Ho, Phys. Rep. **99**, 1 (1983).
- [18] N. Moiseyev, Physics Reports **302**, 212 (1998).
- [19] F. Schöne, S.-O. Krüger, P. Grünwald, M. Aßmann, J. Heckötter, J. Thewes, H. Stolz, D. Fröhlich, M. Bayer, and S. Scheel, Journal of Physics B: Atomic, Molecular and Optical Physics **49**, 134003 (2016).
- [20] F. Schweiner, J. Ertl, J. Main, G. Wunner, and C. Uihlein, Phys. Rev. B **96**, 245202 (2017).
- [21] P. Schmelcher and L. S. Cederbaum, Zeitschrift für Physik D Atoms, Molecules and Clusters **24**, 311 (1992).
- [22] F. Schöne, S.-O. Krüger, P. Grünwald, H. Stolz, S. Scheel, M. Aßmann, J. Heckötter, J. Thewes, D. Fröhlich, and M. Bayer, Phys. Rev. B **93**, 075203 (2016).
- [23] J. W. Hodby, T. E. Jenkins, C. Schwab, H. Tamura, and D. Trivich, Journal of Physics C: Solid State Physics **9**, 1429 (1976).
- [24] O. Madelung, U. Rössler, and M. Schulz, eds., *Landolt-Börnstein - Group III Condensed Matter* (Springer-Verlag, Berlin Heidelberg, 1998).
- [25] E. Anderson, Z. Bai, C. Bischof, S. Blackford, J. Demmel, J. Dongarra, J. Croz, A. Greenbaum, S. Hammarling, and A. McKenney, *LAPACK Users' Guide, Third edition* (Society for Industrial and Applied Mathematics, 1999).
- [26] G. Koster, J. Dimmock, R. Wheeler, and H. Statz, *Properties of the thirty-two point groups*, Massachusetts institute of technology press research monograph (M.I.T. Press, Cambridge, 1963).
- [27] See Supplemental Material, which includes additional numerical data on the green exciton series.
- [28] C. Malerba, F. Biccari, C. Azanza Ricardo, M. D'Incau, P. Scardi, and A. Mittiga, Solar Energy Materials and Solar Cells **95**, 2848 (2011).

SUPPLEMENTAL MATERIAL

In this Supplemental Material we will present additional numerical data for the green exciton series, including an assignment of approximate quantum numbers, group theoretical representations and degeneracies of states. The assignment of approximate quantum numbers is a nontrivial task, due to the strong overlap of n and L manifolds. To this end, starting with the hydrogen-like exciton model, we slowly switch on the band structure and follow the resonance positions. We also apply projection operators to the eigenstates $|\psi\rangle$ to help with the assignment of quantum numbers.

The Hamiltonian of excitons in cuprous oxide in relative coordinates can be separated into the form (see Refs. [4, 14] in the paper).

$$H = E_g + H_0 + H_{\text{SO}} + \lambda H_{\text{vb}}, \quad (1)$$

with the hydrogen-like part

$$H_0 = \frac{\gamma'_1 \mathbf{p}^2}{2m_0} - \frac{e^2}{4\pi\epsilon_0\epsilon|\mathbf{r}|}, \quad (2)$$

using $\gamma'_1 = \gamma_1 + m_0/m_e$, the spin-orbit coupling term

$$H_{\text{SO}} = \frac{2}{3}\Delta \left(1 + \frac{1}{\hbar^2} \mathbf{I} \cdot \mathbf{S}_h\right), \quad (3)$$

and additional terms stemming from the complex valence band structure H_{vb} ,

$$\begin{aligned} H_{\text{vb}} = & \frac{1}{2\hbar^2 m_0} \{4\hbar^2 \gamma_2 \mathbf{p}^2 + 2(\eta_1 + 2\eta_2) \mathbf{p}^2 (\mathbf{I} \cdot \mathbf{S}_h) \\ & - 6\gamma_2 (p_1^2 \mathbf{I}_1^2 + \text{c.p.}) - 12\eta_2 (p_1^2 \mathbf{I}_1 \mathbf{S}_{h1} + \text{c.p.}) \\ & - 12\gamma_3 (\{p_1, p_2\} \{\mathbf{I}_1, \mathbf{I}_2\} + \text{c.p.}) \\ & - 12\eta_3 (\{p_1, p_2\} (\mathbf{I}_1 \mathbf{S}_{h2} + \mathbf{I}_2 \mathbf{S}_{h1}) + \text{c.p.}) \}. \end{aligned} \quad (4)$$

To make possible the assignment of states, we introduce the parameter λ in Eq. (1) controlling the strength of the band structure. For $\lambda = 0$, the excitons are described in the hydrogen-like model and with $\lambda = 1$ the full band structure is switched on. We now diagonalize the Hamiltonian as described in the Paper, while varying λ between zero and one. Following the resonance states in the resulting E - λ -diagram then allows for the assignment of the principal quantum number as shown in Fig. 1. Still, the assignment remains ambiguous due to the existence of various avoided crossings. We additionally calculate the P state component

$$p_P = |\langle L = 1 | \psi \rangle|^2 = \langle \psi | P_{L=1} | \psi \rangle \quad (5)$$

and the F state component

$$p_F = |\langle L = 3 | \psi \rangle|^2 = \langle \psi | P_{L=3} | \psi \rangle \quad (6)$$

with the corresponding projection operators $P_{L=1}$ and $P_{L=3}$, respectively.

In Table I we present the numerical data for all odd parity green resonance states with energies up to $E = 2.299$ eV and dominant P states up to $n = 15$. The table includes the assignment of the approximate principal quantum number n , orbital angular momentum L , irreducible representation, degeneracy g , complex resonance energy E , and the complex relative oscillator strength f_{rel} . Furthermore, we provide the values for p_P and p_F computed according to Eqs. (5) and (6) and the yellow admixture

$$p_Y = |\langle J = 1/2 | \psi \rangle|^2 = \langle \psi | P_{J=1/2} | \psi \rangle. \quad (7)$$

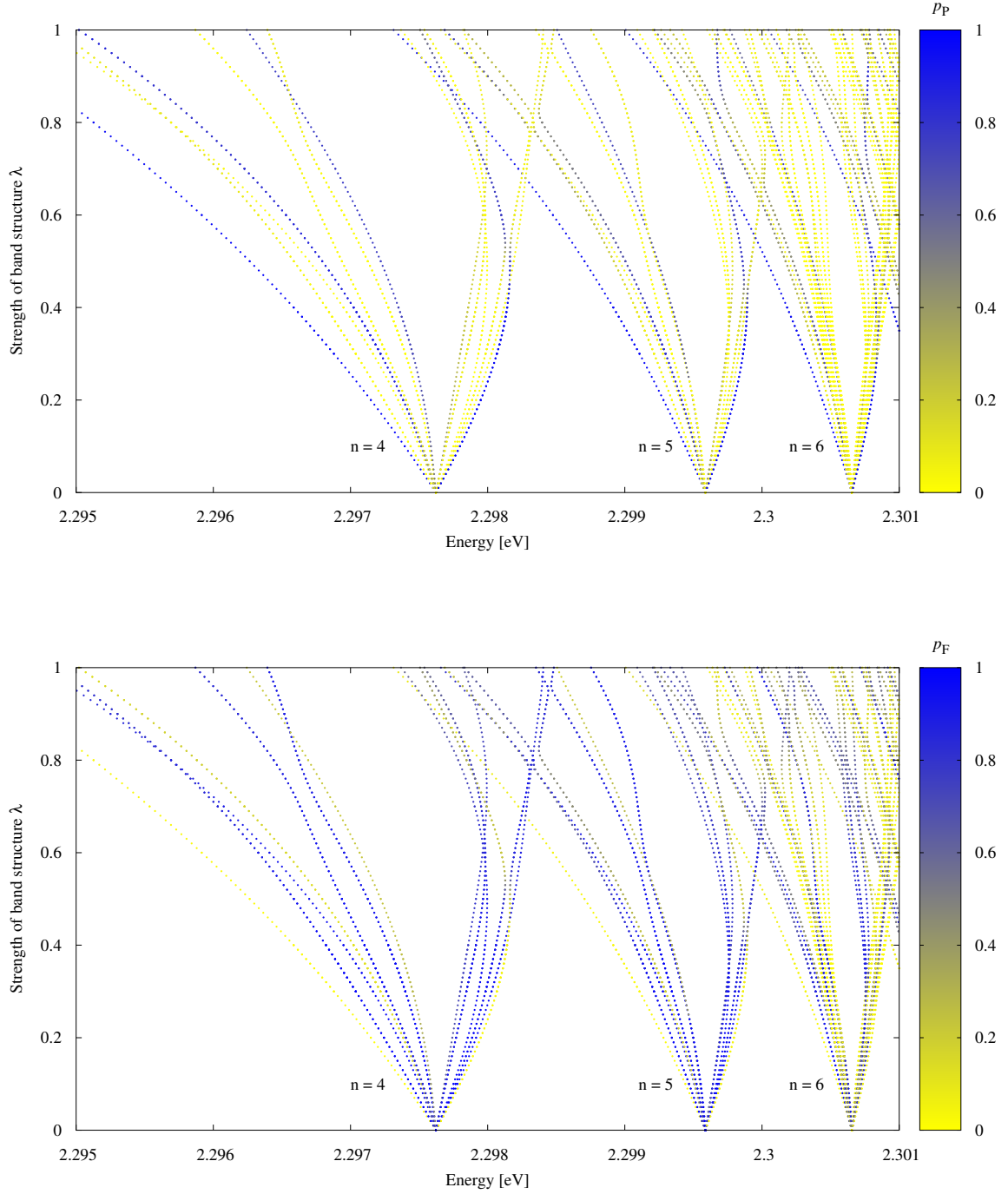


FIG. 1. Energies of states as a function of the strength of the band structure. A value of $\lambda = 0$ means that the band structure is completely switched off, whereas a value of $\lambda = 1$ signifies that the band structure is completely switched on. The color palette shows the P state component p_P (top) and F state component p_F (bottom) given in Eqs. (5) and (6), respectively.

TABLE I. Numerical data for all odd parity green resonance states with energies up to $E = 2.299$ eV and dominant P states up to $n = 15$. The table includes the assignment of the approximate principal quantum number n , orbital angular momentum L , irreducible representation, degeneracy g , complex resonance energy E , and the complex relative oscillator strength f_{rel} . Furthermore, we provide the values for p_{P} and p_{F} computed according to Eqs. (5) and (6) and the yellow admixture p_{y} according to Eq. (7). For one of the 4F states, we could not get a precise value for p_{P} due to convergence problems.

State	Irrep.	g	Re E [eV]	Im E [meV]	Re f_{rel}	Im f_{rel}	p_{P}	p_{F}	p_{y}
2P	Γ_6^-	4	2.26887	-3.01965	4.2998	5.8604	0.955	0.043	0.018
2P	Γ_8^-	8	2.27404	-1.19593	0.7471	1.4121	0.879	0.117	0.010
2P	Γ_7^-	4	2.27948	-0.81870	0.0000	0.0000	0.856	0.136	0.017
2P	Γ_8^-	8	2.28559	-0.04207	-0.0177	0.0146	0.857	0.141	0.004
3P	Γ_6^-	4	2.28765	-0.90691	1.1603	1.8982	0.966	0.030	0.009
3P	Γ_8^-	8	2.28944	-0.39764	0.2350	0.4813	0.895	0.099	0.004
3P	Γ_7^-	4	2.29178	-0.26468	0.0000	0.0000	0.875	0.118	0.007
3P	Γ_8^-	8	2.29384	-0.00734	-0.0052	0.0083	0.611	0.379	0.001
4P	Γ_6^-	4	2.29423	-0.38575	0.5028	0.8270	0.941	0.050	0.004
4F	Γ_6^-	4	2.29474	-0.00149	0.0039	-0.0007	0.030	0.833	0.001
4F	Γ_8^-	8	2.29486	-0.04633	-0.0475	0.0259	0.030	0.842	0.002
4P	Γ_8^-	8	2.29502	-0.13785	0.1574	0.1803	0.885	0.110	0.001
4F	Γ_8^-	8	2.29587	-0.00089	-0.0001	0.0001	0.012	0.824	0.001
4P	Γ_7^-	4	2.29625	-0.12115	0.0000	0.0000	0.769	0.222	0.003
4F	Γ_8^-	8	2.29639	-0.00593	-0.0024	0.0131	0.072	0.905	0.001
5P	Γ_6^-	4	2.29731	-0.19095	0.2571	0.4496	0.905	0.091	0.002
4F	Γ_6^-	4	2.29737	-0.00676	0.0004	-0.0169	~ 0	0.565	0.000
4P	Γ_8^-	8	2.29751	-0.00784	-0.0061	0.0080	0.461	0.476	0.001
4F	Γ_8^-	8	2.29754	-0.00193	-0.0003	0.0025	0.058	0.550	0.000
5F	Γ_6^-	4	2.29766	-0.00303	0.0092	0.0002	0.095	0.788	0.001
5P	Γ_8^-	8	2.29769	-0.08012	0.0503	0.0934	0.748	0.239	0.001
4F	Γ_7^-	4	2.29782	-0.00014	0.0000	0.0000	0.035	0.622	0.000
5F	Γ_8^-	8	2.29783	-0.01073	0.0158	0.0061	0.313	0.596	0.000
5F	Γ_8^-	8	2.29835	-0.00059	-0.0001	0.0000	0.013	0.835	0.001
4F	Γ_7^-	4	2.29841	-0.01880	0.0000	0.0000	0.035	0.896	0.001
4F	Γ_8^-	8	2.29848	-0.00070	0.0006	0.0009	0.097	0.846	0.000
5P	Γ_7^-	4	2.29851	-0.04862	0.0000	0.0000	0.791	0.175	0.001
5F	Γ_8^-	8	2.29875	-0.00545	-0.0017	0.0127	0.090	0.897	0.001
6P	Γ_6^-	4	2.29901	-0.10700	0.1337	0.2630	0.812	0.164	0.001
7P	Γ_6^-	4	2.30005	-0.06821	0.1416	0.1579	0.671	0.275	0.001
8P	Γ_6^-	4	2.30072	-0.04328	0.0519	0.1085	0.648	0.290	0.001
9P	Γ_6^-	4	2.30120	-0.03314	0.0438	0.0730	0.510	0.368	0.000
10P	Γ_6^-	4	2.30154	-0.02334	0.0302	0.0550	0.509	0.383	0.000
11P	Γ_6^-	4	2.30180	-0.01733	0.0268	0.0387	0.455	0.429	0.000
12P	Γ_6^-	4	2.30199	-0.01459	0.0198	0.0322	0.363	0.418	0.000
13P	Γ_6^-	4	2.30215	-0.01012	0.0168	0.0223	0.404	0.462	0.000
14P	Γ_6^-	4	2.30227	-0.00903	0.0118	0.0212	0.327	0.408	0.000
15P	Γ_6^-	4	2.30237	-0.00742	0.0105	0.0165	0.321	0.474	0.000